LA-UR -85-4056

CONF-8509118--2

RECEIVED BY OSTI DEC 06 1985

LA-UR--85-4056

DE86 003660

TITLE: NON-ELASTIC CROSS-SECTIONS FOR NEUTRON INTERACTIONS WITH CARBON AND OXYGEN ABOVE 14 MeV

AUTHOR(S): D. J. Brenner
R. E. Prael

SUBMITTED TO: Proceedings of the IAEA Advisory Group Meeting on Nuclear and Atomic Data for Radiotherapy and Radiobiology (IAEA Panel Proceedings Series) - Sept. 16-20, ~~1986~~ 1985, Radiobiological Institute, T.N. O. Rijswijk, THE NETHERLANDS

Los Alamos Los Alamos National Laboratory
Los Alamos, New Mexico 87545

FORM NO 836 R4
ST NO 2629 5/81

MASTER

Non-Elastic Cross-Sections for Neutron Interactions with Carbon and Oxygen Above 14 MeV

D. J. Brenner
Radiological Research Laboratory
Columbia University
630 West 168th Street
New York, NY 10032, USA

R. E. Prael
Los Alamos National Laboratory
Group X6
Los Alamos, NM 87545, USA

Abstract

In the light of the new generation of high energy (≤ 80 MeV) neutron therapy facilities currently being tested, the need for neutron kerma factors in the range from 15 to 80 MeV on carbon and oxygen has become of urgent importance. Not enough experimental data currently exist or are likely to be measured soon, so a nuclear model is essential for interpolation or, less satisfactorily, extrapolation of available data. The use of a suitable model, applicable to light nuclei, is shown to be crucial. Such a model is described, and good agreement between its results and the experimental data in the energy range of interest is reported. Comparisons between the model predictions and the ENDF/B-V evaluation of the non-elastic cross-section for carbon between 15 and 20 MeV indicate that a re-evaluation of ENDF is required.

Introduction

The use of high energy ($\leq$ 80 MeV) neutron radiotherapy facilities at various centers around the world is beginning to increase [1]. In order that meaningful intercomparisons be made between the different neutron facilities, each with a characteristic neutron energy spectrum, it is essential that the same estimated dose at different facilities should indeed correspond, as precisely as possible, to the same energy deposition per unit mass of tissue. This requirement in turn necessitates a precise knowledge of neutron kerma factors and ratios over the energy range of interest [2].

However, due to lack of nuclear data above 14 MeV, only kerma factors for hydrogen are known with acceptable precision (a few percent). The other two elements of importance, carbon and oxygen, have considerable uncertainties, due to our lack of knowledge of detailed cross-sections for the various possible neutron-induced reactions.

To rectify this situation a large amount of nuclear data is required. It is not sufficient, for example, to know the total cross-section for a particular reaction, for the kerma factor refers to the energy of emitted secondary particles. Thus, detailed reaction mechanisms or, equivalently, complete secondary charged particle spectra, must be known. It is not practical to expect complete data of this type to become experimentally available over the whole energy range of interest ($14 < E_n < 80$); this is in part because of difficulties in measurement techniques and beam availability, but also because

of the enormous expense that would be involved. A more practical possibility, therefore, is to develop model calculational techniques, which have been validated by whatever nuclear data are available in the energy range of interest, and serve ideally to interpolate (but sometimes of necessity to extrapolate) the experimental data that do exist. It is the purpose of this contribution to describe such a technique.

Appropriate and Inappropriate Approaches

As described above, the calculations must agree with such experimental data that are available: we are concerned here with non-elastic neutron cross-sections for the light nuclei carbon and oxygen. As described in an earlier review [3], the nature of these light nuclides is such that their unique nuclear structures must be taken into account in any model calculation, as the effects of their structures are not masked by the statistical behavior caused by a large number of nucleons. In addition, of course, both carbon and oxygen exhibit considerable alpha-particle clustering: for example, the calculations of Kurath [4] and Balashov et al. [5] both indicate large spectroscopic factors for alpha particles in carbon and oxygen; also, experimentally there is some evidence from alpha transfer and knockout reactions, in carbon and oxygen, that there is considerable alpha clustering [6].

These considerations then, lead us to conclude that a 'general purpose' nuclear reaction model--of which several exist--will not be appropriate for light nuclei. Further

evidence to support this thesis will be given from our own calculations below, but for the moment, we illustrate the point by reference to some data from the literature.

The de-excitation by particle emission of excited compound nuclei is usually calculated using a statistical evaporation model, first described by Weisskopf [7] in which the probability that an excited nucleus with excitation E_c will emit a particle with energy E is proportional to $E\omega(E_c - E)$, where $\omega(E_c - E)$ is the density of energy levels of the residual nucleus at excitation $E_c - E$. The analytic form of the density of levels is usually taken to be [8]

$$\omega(\varepsilon) \sim \exp\left(2\sqrt{a(\varepsilon-\delta)}\right) , \qquad (1)$$

where a is a constant for a given nucleus and δ is the pairing energy. From such considerations, Le Couteur [9] calculated that the energy spectrum of evaporated particles to be proportional to

$$E^{\frac{5}{11}} \, c^{\frac{-12F}{11T}} , \qquad (2)$$

where T is the initial nuclear 'temperature'. Thus, a logarithmic plot of the production cross-section for low energy (evaporated) secondary particles, divided by $E^{\frac{5}{11}}$ should yield a straight line. Such a representation, taken from the work of Cross [10], for the production of low energy secondary neutrons from 190-MeV proton bombardment of various nuclides, is shown in

Figure 1. It can be seen that for the heavier nuclei, Equation (2) does seem to apply, but the agreement becomes progressively worse as the target mass decreases, and is very poor for carbon. This may be understood by reference to Figure 2, where the energy levels for a light nucleus and a heavy nucleus are compared. It is clear that the use of an analytic form such as Equation (2) to describe the density of energy levels, whilst potentially reasonable for gold, is entirely inappropriate for a nucleus such as carbon, which has its own unique, and not-analytically describable, energy levels.

Having established that whatever model is to be used, it must specifically take into account the special properties of light nuclei, we consider what might be an appropriate model. It has been clear for about 40 years that the angle and energy of particles coming out of a high energy nuclear reaction result from a two-step process [11]. In the first 'direct' stage, the incident particle energy is shared progressively amongst more and more degrees of freedom of the system. In other words the incident particle makes collisions with individual nucleons or groups of nucleons within the nucleus and these, in turn, have further collisions in the same nucleus, generating an intra-nuclear cascade. Some of the products of such collisions may acquire sufficient energy to escape from the nucleus, these high energy particles being referred to as 'direct' products, being predominantly emitted in the forward direction. In the second, 'equilibrium' stage, the remaining energy is statistically

distributed in a compound nucleus and results in the emission of lower energy particles, isotropic in the center of mass system.

For the first intra-nuclear cascade part of the reaction, we follow the technique first suggested by Goldberger [12]. Here the target nucleus is treated as a degenerate Fermi gas, and the nucleon-nucleon or nucleon-cluster collisions within the nucleus are determined by experimentally determined free (i.e., on-shell) differential cross-sections. The path of these nucleons and clusters is then traced by Monte-Carlo techniques, i.e., sampling distributions based on these on-shell cross-sections together with assumptions about nuclear density and nucleon or cluster momenta. All primary and secondary particles are followed until either they escape from the nucleus or their energy becomes small.

Our particular implementation of the Goldberger technique will be described in the next section. It is worthwhile, however, to mention briefly the inherent assumptions of the technique.

Firstly, in order to use the two-body interaction model for each collision in the cascade, the average intranuclear mean free path should be larger than the wavelength of the particles in the cascade. Roughly, this appears to be the case at particle energies of about 100 MeV and above, though the rapidity and degree of breakdown of the model below 100 MeV is not known, and can only really be evaluated by detailed comparison with experiment. Secondly, the use of experimentally determined nucleon-nucleon and nucleon-cluster cross-sections

implies that the off-shell interaction matrix elements inside the nucleus can be approximated by on-shell values: the separation energy of an alpha cluster in carbon or oxygen is only about 7 MeV; however, for nucleons, it varies from 12 to 19 MeV. These rather large nucleonic separation energies might imply that free nucleon-nucleon cross-sections are not completely appropriate; however, the magnitude of this effect is difficult to assess a priori.

The Intranuclear Cascade Code, INCA1

Our intranuclear cascade code is based on the one described by Chen et al. [13], although without provision for pion production, implying an upper energy limit of around 300 MeV. It allows for a description of the nucleus in terms of nucleons, alpha clusters and two-nucleon clusters. (The two-nucleon clustering is for a description of ^{14}N.) We have taken spectroscopic factors--the measure of finding a cluster in the nucleus--from the work of Balashov et al. [5], whose calculations in turn agree with the results of cluster 'knockout' experiments on carbon and oxygen. For example, the ^{16}O nucleus is taken to be a time average of 2.52 alpha clusters plus 5.92 nucleons, whilst the ^{12}C nucleus is taken to be represented by 1.64 alpha clusters plus 5.44 nucleons. The nucleus is assumed to be spherically symmetric and to consist of a series of 18 annular spherical shells, each with a density obtained from two- or three-parameter Fermi distributions derived from electron elastic scattering [14]. In each shell Fermi-momentum distri-

butions for nucleons are calculated, based on the nucleon density in that region. For the clusters, which are bosons, a Fermi momentum distribution appropriate to the density normalized to a single particle is used. For nucleon scattering, Pauli blocking is enforced, such that a collision is only allowed if both nucleons have a final energy greater than their Fermi energies. Particle emission is restricted by one and two particle separation energies, which are updated on a time-dependent basis to take into account prior particle emissions, and to ensure energy conservation. Finally, particles are allowed to escape freely when their radial position approximately exceeds the half-density radius of the nucleus.

We have also included a simple model for nucleon transfer, in particular, the nucleon pickup reaction yielding the deuteron, a process known to contribute significantly to the charged particle yield [15]. In the spirit of the intra-nuclear cascade we have followed the conceptual approach used in Ref. 15, whereby on-shell transfer cross-sections were successfully used. As a first approach, these transfer cross-sections are estimated using the plane-wave Born approximation as described by Selove [16].

When no further direct emission is energetically possible, the type, energy and direction of all emitted particles and the compound nucleus are recorded, and another incident particle treated. Typically 10^5 incident particles are used for INCA1, taking, for oxygen at 20 MeV, around 1 hour on a CRAY X-MP

computer. The compound nuclei are then allowed to decay by 'Fermi-breakup' as described in the next section.

Fermi Breakup of the Compound Nucleus, INCA2

As discussed above, the use of an evaporation model to describe the particle emission from an equilibrium compound nucleus is not realistic for light nuclei. Therefore, we use an approach, termed 'Fermi breakup', suggested initially by Fermi [17], and subsequently used by, among others, Zhdanov and Fedotov [8] and Gradsztajn et al. [19]. Fermi pointed out that if the energy of the collision is dumped into a small nuclear volume, it will be rapidly statistically redistributed among the degrees of freedom of the system. This conclusion will be true independent of the number of particles in the volume. All possible final states will then appear with frequencies proportional to their statistical weights which, excluding spin factors, will be

$$S_n \propto \frac{dQ(w)}{dw} = \int \prod_1^n d\vec{p}_i \ , \qquad (3)$$

for a state of n non-relativistic particles with momenta $\vec{p}_i$. Here Q is the volume of phase space corresponding to the total energy, w. This integral, with the constraints of energy and momentum conservation, was calculated analytically--though incorrectly--by Rozental [20], and subsequently by Brenner [21]:

$$\frac{dQ}{dw} = \frac{2\pi^{\frac{3n-3}{2}}}{\Gamma(\frac{3n-3}{2})} \left[\frac{\prod_1^n \mu_n}{\sum_1^n \mu_n} \right]^{\frac{1}{2}} T^{\frac{3n-5}{2}} , \qquad (4)$$

where T is the total kinetic energy and μ_i the mass of particle i. Thus, the breakup probability for all possible channels may be computed, and a particular channel chosen by random-number techniques.

In contrast to earlier implementations of the Fermi breakup technique, we have recognized that a considerable number of decays go through particle-unstable intermediate states, and we have thus allowed multiple, sequential decays.

Some other novel features of INCA2 are the use of a Coulomb barrier penetration factor, derived from Coulomb wave functions, for two-body breakup (the most common type); for multi-particle breakup, a simple threshold is used, adjusted for Coulomb energy. Again for the most commonly found two-body breakup, parity and isospin conservation is enforced, as well as a restriction of particle emission by a neutral-particle angular momentum barrier. For carbon and oxygen in the range below about 100 MeV, eight-body breakup is sufficiently unlikely to allow restriction of calculating probabilities only up to seven-body breakup. If much higher energies are required, the code could be extended, though with an increase in running time.

Finally, and very importantly, up-to-date experimental data are used as the data-base for mass excesses, excitation

energies, spins, isospins, and parities of all available nuclear levels.

Comparison of INCA Results with Experiment

As discussed above, the utility of a nuclear model as an interpolating or, less ideally, extrapolating device for available nuclear data depends on a detailed comparison with experiment where it is available. By far the most detailed experimental data available in the energy range of interest are the results of measurements of double-differential hydrogen and helium spectra produced by neutron reactions on carbon, nitrogen and oxygen at 27.4, 39.7 and 60.7 MeV. For carbon, a comparison has been published elsewhere [22], so only a few pertinent details will be discussed here. (For oxygen, similar comparisons are currently being undertaken, preliminary results indicating a degree of agreement similar to that for carbon.) When evaluating these comparisons, it should be born in mind that the INCA model does not have any free parameters, so the calculation is in no sense a 'fit' to the data.

Figures 3 and 4 show some typical comparisons for carbon at 27.4 and 60.7 MeV incident neutron energy, at various angles. Also shown in these figures are the charge-symmetric proton-induced data measured by Bertrand and Peelle [23] at the same energies. Overall, the agreement for all particle types is quite satisfying.

Figure 5 illustrates the effects of not treating the particular properties of the light nuclei correctly. The short-

dashed lines are the results of INCA runs where a) the spectroscopic factor for α-clustering was set to zero, and b) the cross-section for deuteron pickup was set to zero. It is clear that the yield of deuterons and alphas--which together (see below) are responsible for almost half the total kerma--is not reproduced in this case.

The results of this comparison give great confidence in the model at energies above 27 MeV. Between this energy and 15 MeV--where presumably the model will become increasingly less realistic--no such complete experimental data are available. However, a recent emulsion experiment [25] has the potential to yield more limited, but in some cases more specific, data. This work involves an incident spectrum of neutron energies impinging on an emulsion containing carbon, nitrogen, oxygen and silver. If the final state contains no more than one neutral particle, the reaction can in principle be uniquely identified, and further Dalitz-plot analysis can also reveal intermediate states for particular reactions. This approach was used to measure the cross-sections for the reaction $^{12}C(n,n')3\alpha$ between 11 and 35 MeV. Circuitously, however, such an approach requires corrections for phenomena such as three-pronged events not caused by three alphas, and reactions in which an alpha is not detected as it is below the detection threshold in the emulsion: such corrections, of course, presuppose the measurements in question. Our INCA codes appear to be an ideal tool for such corrections and when applied to the data, as discussed in Ref. 26, yield cross-sections 10 to 30% lower than originally

reported. Figure 6 shows a comparison of the revised data with INCA predictions for the $^{12}C(n,n')3\alpha$ reaction.

Dalitz-plot analysis of emulsion data can also yield partial cross-sections, and comparison with calculations then becomes a particularly sensitive test of the model. Figure 7 shows a comparison of the revised emulsion data for the $^{12}C(n,n')^{12}C^*(9.63MeV)\rightarrow 3\alpha$ reaction, with INCA results, and also with some recent time-of-flight measurements at 20 to 26 MeV [27].

This latter time-of-flight experiment also reported cross-sections for the $^{12}C(n,n')^{12}C^*(4.43MeV)$ reaction, which are compared with INCA predictions in Table I.

Overall, then, it appears that satisfactory agreement between theory and experiment exists in the 14 to 65 MeV range. One exception is the recent time-of-flight measurement of the $^{12}C(n,n')3\alpha$ cross-section at 14 MeV [28], yielding 110 ± 15 mb. This is in total disagreement with other experimental measurements at this energy (230, 287, 230 mb) and with our calculations (262 mb). The discrepancy is extremely large and should be investigated further.

Predicted Reaction Mechanisms at 20 MeV

There is currently much debate over not only the reaction cross-sections for neutron interactions on light nuclei, but also the reaction mechanisms. In this section, we show some predictions for carbon and oxygen at 20 MeV. In the light of the comparisons in the previous section, these results are

clearly predictive of the basic reaction mechanism features though, based on those comparisons, the actual branching ratios are estimated to have an uncertainty, due to the model, of up to about 25%.

Table II shows the yield of compound nuclei, at the point where all direct emission has ceased, but no breakup of compound nuclei has occurred. It can be seen that the most common outcome of the direct reaction is the emission of one neutron, or no emission at all; however, as seen in Figure 5, the direct emission of charged particles is certainly significant and increasingly so with increasing energy. The mechanisms for the breakup of $^{12}C^*$ and $^{13}C^*$ are shown in Figures 8 and 9. The lowest excited state of ^{12}C simply decays by gamma emission, but the higher states mostly decay by sequential two-body decays to yield 3α. The decay of ^{13}C is much more complex; for clarity, decays leading to $3\alpha + n$ (the majority) have been displayed separately from those leading to other final states. Table III sums up those mechanisms that lead to the $^{12}C(n,n')3\alpha$ reaction at 20 MeV. Only those channels with cross-sections more than 1% of the total are shown, but even with this restriction there are 13 distinct mechanisms--a difficult situation for an analytic calculation! As the energy increases, so the number of channels increases.

Table IV shows the yield of compound nuclei at the equilibrium stage after 20-MeV neutrons are incident on oxygen. Figures 10 and 11 then show the mechanisms for the decay of the

predominant compound nuclei $^{16}O^*$ and $^{17}O^*$. Again, the diversity of reactions is notable.

Perusal of these figures reveals an interesting contrast between carbon and oxygen at 20 MeV. Whilst for carbon, almost all (99%) the yield of alphas is from multiple alpha emission, 85% of the alpha yield of oxygen is from single alpha emission. As more channels open at higher energies, this contrast decreases, and at 35 MeV, only 35% of the alpha yield is from single alphas. Such considerations are, of course, of considerable microdosimetric importance.

Comparisons with ENDF for Carbon

The latest evaluation of neutron cross-sections in carbon was undertaken in 1978 by Fu and Perey for ENDF/B-V [29]. The non-elastic cross-section above 14 MeV was estimated by subtracting the elastic from the total cross-section; evaluation of the predominant alpha-production cross-section was apparently guided by this and by the old emulsion data of Frye et al. [30] and Vasilev et al. [31], illustrated in Figure 6. The evaluated alpha production is shown in Figure 12, together with the INCA prediction. Comparison with Figure 6 illustrates that the large rise in the evaluated alpha-production cross-section appears to be based on two data points by Vasilev et al. [31], at 17 and 18 MeV, each with over 30% error bars, and which have had rather uncertain corrections made for low-energy alphas that were not detectable in the emulsion.

Table V illustrates that such a massive rise in the α-pro-

duction and thus the non-elastic cross-section is not necessarily implied by the most recently available elastic [27,32] and total [33] cross-sections. Both at 14 and 20 MeV, the INCA predictions are consistent with the available data. This, together with the results of the more recent emulsion experiment, indicate that the non-elastic cross-section is probably continuously decreasing above 15 MeV.

Kerma Factors

The INCA codes are capable of predicting only non-elastic and compound-elastic cross-sections. Shape-elastic cross-sections, which, at 14 MeV, contribute about 30% and 20% to the total kerma for carbon and oxygen respectively (decreasing to about 5% at 60 MeV), must be estimated separately. Above 14 MeV, appropriate data are sparse and optical model analyses of available data such as those reported in Refs. 27 and 34 must of necessity be considered rather uncertain. For example, in Ref. 27 at 40 MeV, the kerma factor for elastic scattering of carbon derived directly from the data, and derived from the best optical model fit to the same data, differ by about 10%! In part this is due to the fact that, because of the energy weighting in the definition of kerma, middle and back angles which have smaller cross-sections and tend not to be measured so well (if at all), make the largest contribution to the kerma factor. The situation appears even worse for oxygen, where it seems to be the case that (cf Ref. 35), at least in the energy range from 20 to 26 MeV, there is a deep back-angle minimum at around 120°

that cannot be reproduced by any conventional parameterisation of the spherical optical potential.

With these caveats, Equation (5) and Table VI show fits to our calculated kerma factors, included our best estimate of elastic scattering. Further details and comparisons with other works can be found in Ref. 34.

$$K(E) = p_1 + p_2 E - p_3 \exp(-p_4 E) , \qquad (5)$$

where E is the neutron energy in MeV, and K is the kerma factor in 10^{-18} Gy m^2. The formula was fitted to our predictions between 16 and 80 MeV.

Conclusions

We conclude firstly that a nuclear model is essential to interpolate what experimental data that do exist, in order to calculate non-elastic kerma factors for carbon and oxygen. Secondly, we have argued that a nuclear model must be specific to light nuclei. Such a model has been described and fits well with experimental double-differential secondary charged particle spectra for incident neutrons between 27 and 60 MeV on carbon and oxygen. The model has essentially no free parameters. It also fits reasonably well with the limited data available between 15 and 27 MeV.

Given that the model has been shown to be reasonably reliable, we have argued that the ENDF/B-V evaluation of non-elastic cross-sections and α-production cross-sections for

carbon must be in considerable error between 15 and 20 MeV, perhaps by as much as 30% at some energies. It is in urgent need of re-evaluation.

Finally, kerma factors based on our model calculations are given for carbon and oxygen and tissue. More elastic scattering data and modelling, particularly for oxygen between 15 and 25 MeV, are, however, required to improve these predictions.

Acknowledgement

This investigation was in part supported by Contract DE-AC02-83ER60142 from the US Department of Energy and by PHS Grant CA 15307 awarded by the National Cancer Institute, DHHS, to the Radiological Research Laboratory.

References

[1] SUTTON, C., New Scientist 1474 (1985) 40.

[2] AUSCHALOM, M., ROSENBERG, I., MRAVCA, A., Med. Phys. 10 (1983) 395.

[3] JACKSON, D.F., BRENNER, D.J., Prog. Part. Nucl. Phys. 5 (1981) 143.

[4] KURATH, D., Phys. Rev. C 7 (1973) 1390.

[5] BALASHOV, V.V., BOYARKINA, A.N., ROTTER, I., Nucl. Phys. 59 (1964) 417.

[6] ROOS, P.G., CHANT, N.S., COWLEY, A.A., GOLDBERG, D.A., HOLMGREN, H.D., WOODY, R., Phys. Rev. C 15 (1977) 57.

[7] WEISSKOPF, V.F., Phys. Rev 52 (1937) 295.

[8] BLATT, J.M., WEISSKOPF, V.F., "Theoretical Nuclear Physics", Wiley & Sons, New York (1952).

[9] LE COUTEUR, K.J., Proc. Phys. Soc. 65 (1952) 718.

[10] GROSS, E., The Absolute Yield of Low-energy Neutrons from 190-MeV Proton Bombardment of Gold, Silver, Nickel, Aluminum and Carbon, Univ. of CA Rep. UCRL-3330 (1956).

[11] SERBER, R., Phys. Rev. 72 (1947) 1114.

[12] GOLDBERGER, M.L., Phys. Rev. 74 (1948) 1269.

[13] CHEN, K., FRAENKEL, Z., FRIEDLANDER, G., GROVES, J.P., MILLER, J.M., SHIMAMOTO, Y., Phys. Rev. 166 (1968) 949.

[14] DE JAGER, C.W., DE VRIES, H., DE VRIES, C., At. Data Nucl. Data Tables 14 (1976) 479.

[15] HACHENBERG, F., CHIANG, H.C., HÜFNER, J., Phys. Lett. 97B (1980) 183.

[16] SELOVE, W., Phys. Rev. 101 (1956) 231.

[17] FERMI, E., Prog. Theor. Phys. 5 (1950) 570.

[18] ZHDANOV, A.P., FEDOTOV, P.I., Sov. Phys. JETP 18 (1964) 313.

[19] GRADSZTAJN, E., YIOU, F., KLAPISCH, R., BERNAS, R., Phys. Rev. Lett. 14 (1965) 436.

[20] ROTENTAL, I.L., Sov. Phys. JETP 1 (1955) 166.

[21] BRENNER, D.J., "Pion Interactions with Light Nuclei and Applications to Radiotherapy", Rutherford Laboratory Report, RL-79-032 (1979).

[22] SUBRAMANIAN, T.S., ROMERO, J.L., BRADY, F.P., WATSON, J.W., FITZGERALD, D.H., GARRETT, R., NEEDHAM, G.A., ULLMANN, J.L., ZANELLI, C.I., BRENNER, D.J., PRAEL, R.E., Phys. Rev. C 28 (1983) 521.

[23] BERTRAND, F.E., PEELLE, R.W., Phys. Rev. C 8 (1973) 1045.

[24] DIMBYLOW, P.J., Phys. Med. Biol. 25 (1980) 637.

[25] ANTOLKOVIC, B., SLAUS, I., PLENKOVIC, D., MACQ, P., MEULDERS, J.P., Nucl. Phys. A394 (1983) 87.

[26] BRENNER, D.J., PRAEL, R.E., Nucl. Sci. Eng. 88 (1984) 97.

[27] MEIGOONI, A.S., PETLER, J.S., FINLAY, R.W., Phys. Med. Biol. 29 (1984) 643.

[28] HAIGHT, R.C., GRIMES, S.M., JOHNSON, R.G., BARSCHALL, H.H., Nucl. Sci. Eng. 87 (1984) 41.

[29] KINSEY, R., ENDF/B Summary Documentation, Brookhaven National Laboratory Report BNL-NCS-17541 (ENDF-201) (1979).

[30] FRYE, G.M., ROSEN, L., STEWART, L., Phys. Rev. 99 (1955) 1375.

[31] VASILEV, S.S., KONAROV, V.V., POPOVA, A.M., Sov. Phys. JETP 6 (1958) 1016.

[32] HAOUAT, G., LACHKAR, J., SIGAUD, J., PATIN, Y., COCU, F., Nucl. Sci. Eng. 65 (1978) 331; GLASGOW, D.W., et al., Nucl. Sci. Eng. 61 (1976) 521.

[33] LISOWSKI, P.W., MOORE, M.S., MORGAN, G.L., SHAMU, R.E., "Total Neutron Cross-Sections at WNR", NBS Special Publication SP-594, Washington, DC (1980).

[34] BRENNER, D.J., Phys. Med. Biol. 29 (1984) 437.

[35] PETLER, J.S., ISLAM, M.S., FINLAY, R.W., DIETRICH, F.S., Phys. Rev. C32 (1985) 673.

Table I. Cross Sections for $^{12}C(n,n')^{12}C(2^+)$ 20-26 MeV.

Energy MeV	Experiment [27] mb	INCA/FB mb
20	92	96
24	79	79
26	73	63

Table II.
Intermediate Yield of Compound Nuclei (20-MeV Neutrons on Carbon).

$n + {}^{12}C \rightarrow {}^{13}C^*$	117mb	26%
$\rightarrow {}^{12}C^* + n$	279mb	61%
$\rightarrow {}^{12}B^* + p$	18mb	4%
$\rightarrow {}^{11}B^* + d$	24mb	5%
$\rightarrow {}^{9}Be^* + \alpha$	6mb	1%
$\rightarrow {}^{8}Be^* + \alpha + n$	12mb	3%

Table III
Mechanisms of $^{12}C(n,n')3\alpha$ at 20 MeV.

$n + {}^{12}C$	$\rightarrow n + {}^{12}C^* \rightarrow \alpha + {}^{8}Be \rightarrow 2\alpha$	58%
	$\rightarrow {}^{13}C^* \rightarrow {}^{5}He + {}^{8}Be \rightarrow n + \alpha + 2\alpha$	13%
	$\rightarrow {}^{13}C^* \rightarrow n + {}^{12}C^* \rightarrow \alpha + {}^{8}Be \rightarrow 2\alpha$	6%
	$\rightarrow {}^{13}C^* \rightarrow \alpha + {}^{9}Be^* \rightarrow n + {}^{8}Be \rightarrow 2\alpha$	5%
	$\rightarrow n + \alpha + {}^{8}Be \rightarrow 2\alpha$	5%
	$\rightarrow {}^{13}C^* \rightarrow \alpha + {}^{9}Be^* \rightarrow \alpha + {}^{5}He \rightarrow \alpha + n$	4%
	$\rightarrow {}^{13}C^* \rightarrow \alpha + {}^{9}Be^* \rightarrow n + 2\alpha$	2%
	$\rightarrow {}^{13}C^* \rightarrow 2\alpha + {}^{5}He \rightarrow n + \alpha$	2%
	$\rightarrow n + {}^{12}C^* \rightarrow 3\alpha$	1%
	$\rightarrow {}^{13}C^* \rightarrow n + \alpha + {}^{8}Be \rightarrow 2\alpha$	1%
	$\rightarrow \alpha + {}^{9}Be^* \rightarrow n + {}^{8}Be \rightarrow 2\alpha$	1%
	$\rightarrow \alpha + {}^{9}Be^* \rightarrow \alpha + {}^{5}He \rightarrow \alpha + n$	1%
	$\rightarrow \alpha + {}^{9}Be^* \rightarrow n + 2\alpha$	1%

Table IV
Intermediate Yield of Compound Nuclei (20-MeV Neutrons on Oxygen).

$n + {}^{16}O$	$\rightarrow {}^{17}O^*$	150mb	25%
	$\rightarrow {}^{16}O^* + n$	310mb	52%
	$\rightarrow {}^{16}N^* + p$	31mb	5%
	$\rightarrow {}^{15}N^* + d$	67mb	11%
	$\rightarrow {}^{15}N^* + np$	9mb	2%
	$\rightarrow {}^{13}C^* + \alpha$	17mb	3%
	$\rightarrow {}^{12}C^* + \alpha n$	14mb	2%

Table V
Evaluated Experimental Total and Elastic Cross-Sections (in Barns) for Neutrons on Carbon, Compared with INCA Non-Elastic Predictions.

	Total	Elastic	INCA Non-Elastic
14 MeV	1.32 ± .02	.86 ± .06	.47
20 MeV	1.48 ± .06	.95 ± .10	.46

Table VI. Parameters for Equation (5). The results are valid from 16 to 80 MeV and yield kerma per unit fluence values in 10^{-15} Gy m^2.

	^{1}H	^{12}C	^{14}N	^{16}O	ICRU muscle
p_1	51.79	2.355	12.082	2.730	6.587
p_2	-0.2563	0.03886	-0.02656	0.03085	0.01877
p_3	-0.04246	7.990	11.325	3.532	4.683
p_4	-0.06	0.1445	0.01211	0.05828	0.1314

Figure Captions

1) Low Energy Neutrons emitted after bombardment of various targets by 190-MeV protons [10]. In this representation, if Equation (2) is valid, the data should fall on straight lines.

2) Energy levels of the compound nuclei of ^{13}C and ^{198}Au. Note the energy scale for ^{198}Au has been expanded by about 25 compared with that of ^{13}C.

3) Yield of hydrogen and helium isotopes after bombardment of carbon by 27.4-MeV neutrons. The rows A,B,C,D,E correspond to production angles of 15°, 35°, 65°, 90° and 130°. The points are results of a measurement [22], the histograms are the predictions of the INCA code and the smooth curves are the results of a measurement of the charge-symmetric proton-induced reaction [23].

4) As Fig. 3, for 60.7-MeV incident neutrons. The rows A,B,C,D,E correspond to production angles of 20°, 40°, 65°, 90° and 150°.

5) Comparison of predictions for incident 60.7-MeV neutrons (at 20°) when α-clustering and deuteron pickup are included (full histograms) and when excluded (dashed histograms). The measured data are shown as points.

6) Cross-section for the $^{12}C(n,n')3\alpha$ reaction. The open circles are the results of an emulsion experiment [25], as revised in Ref. [26]. The squares and crosses are, respectively, the results of the emulsion experiments reported in Refs. [30] and [31]. The curve is the prediction of the INCA code.

7) Cross-section for the $^{12}C(n,n')^{12}C^*(9.63MeV)\rightarrow 3\alpha$ reaction. The triangles are the results of the emulsion experiment [25] as revised in Ref. [26]. The circles are the results of a recent time-of-flight measurement [27]. The curve is the prediction of the INCA code.

8) Predicted decay scheme for $^{12}C^*$ formed by bombardment of carbon by 20-MeV neutrons.

9) As Fig. 8 for $^{13}C^*$. The numbers are cross-sections in mb.

10) Predicted decay scheme for $^{16}O^*$ formed by bombardment of oxygen by 20-MeV neutrons. The numbers are cross-sections in mb.

11) As Fig. 10 for $^{17}O^*$.

12) Alpha production cross-section for neutrons incident on carbon. The full curve is the prediction of the INCA code; the dashed curve is the ENDF/B-V evaluation [29].

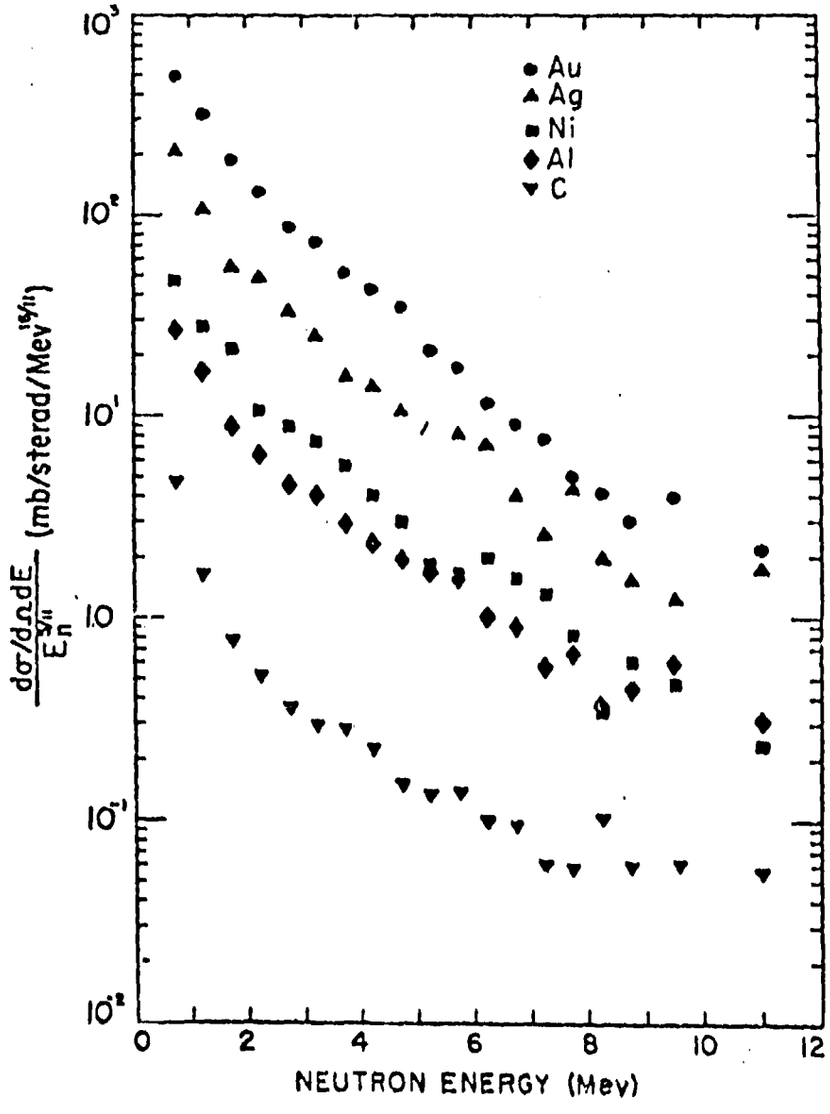
Au
Ag
Ni
Al
C
10^3
10^2
10^1
10
10^{-1}
10^{-2}
$\frac{d\sigma/d\Omega dE}{E_n^{3/2}}$ (mb/sterad/Mev$^{3/2}$)
0
2
4
6
8
10
12
NEUTRON ENERGY (Mev)

Fig 1

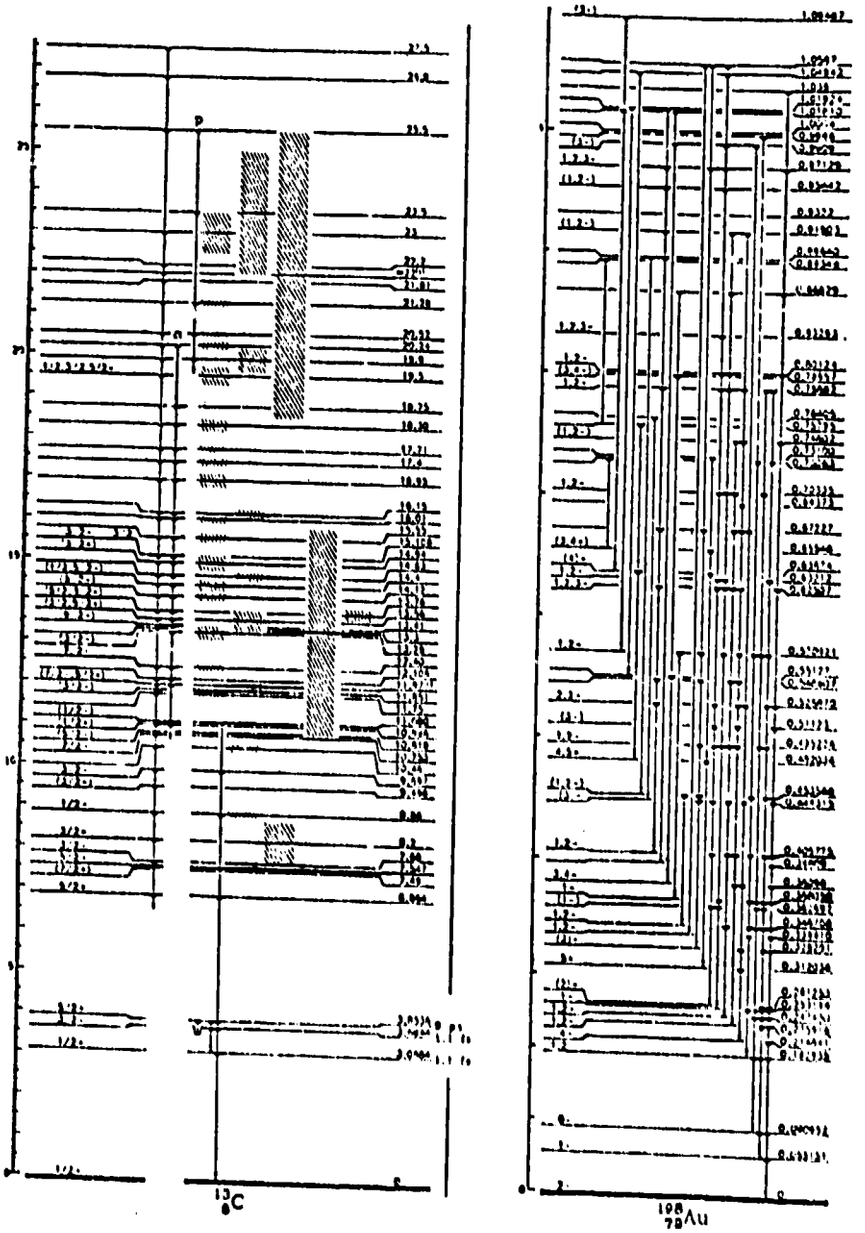

Fig 2

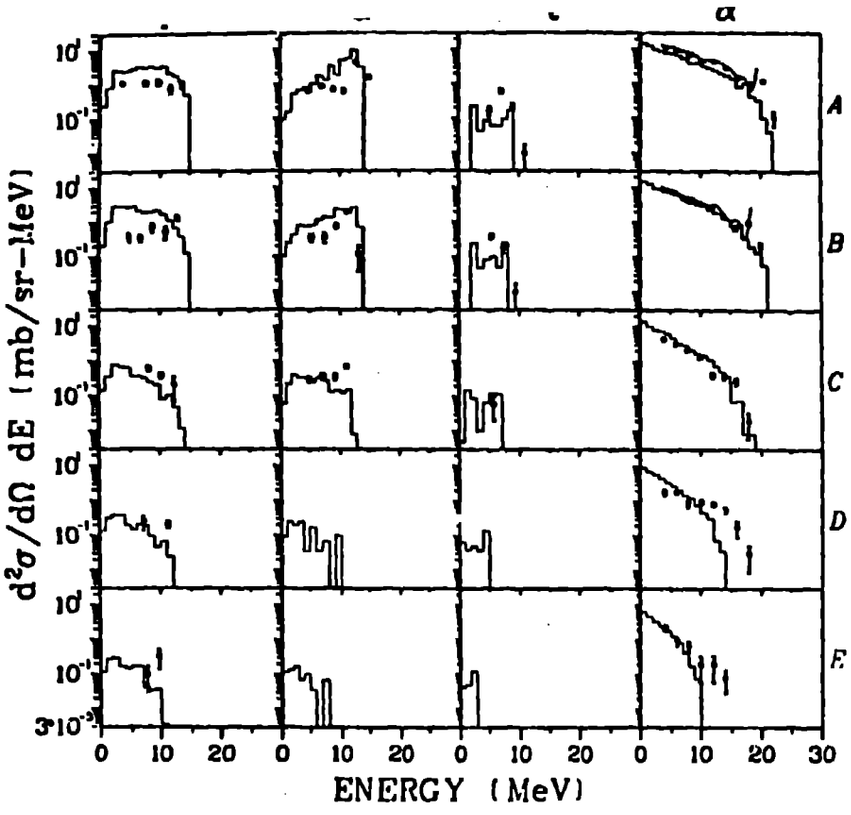
α
A
B
C
D
E
$d^2\sigma/d\Omega\ dE$ (mb/sr-MeV)
ENERGY (MeV)

Fig 3

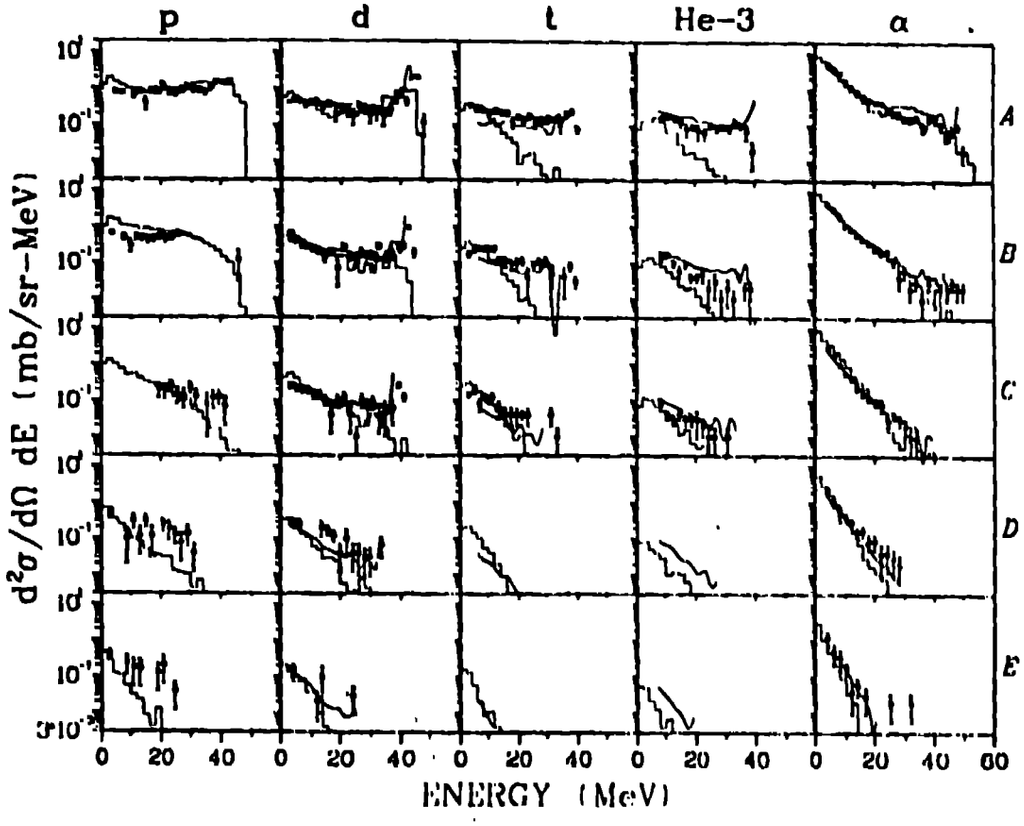
p
d
t
He-3
α
A
B
C
D
E
$d^2\sigma/d\Omega\ dE$ (mb/sr-MeV)
ENERGY (MeV)

Fig 4

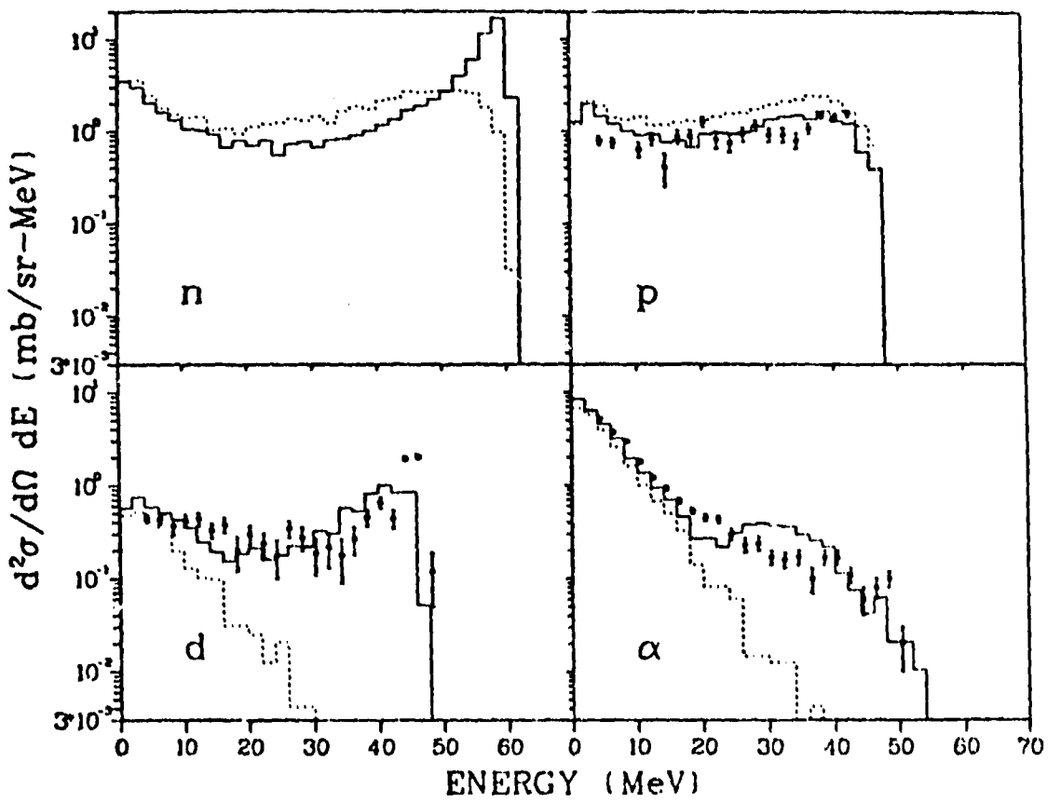

Fig 5

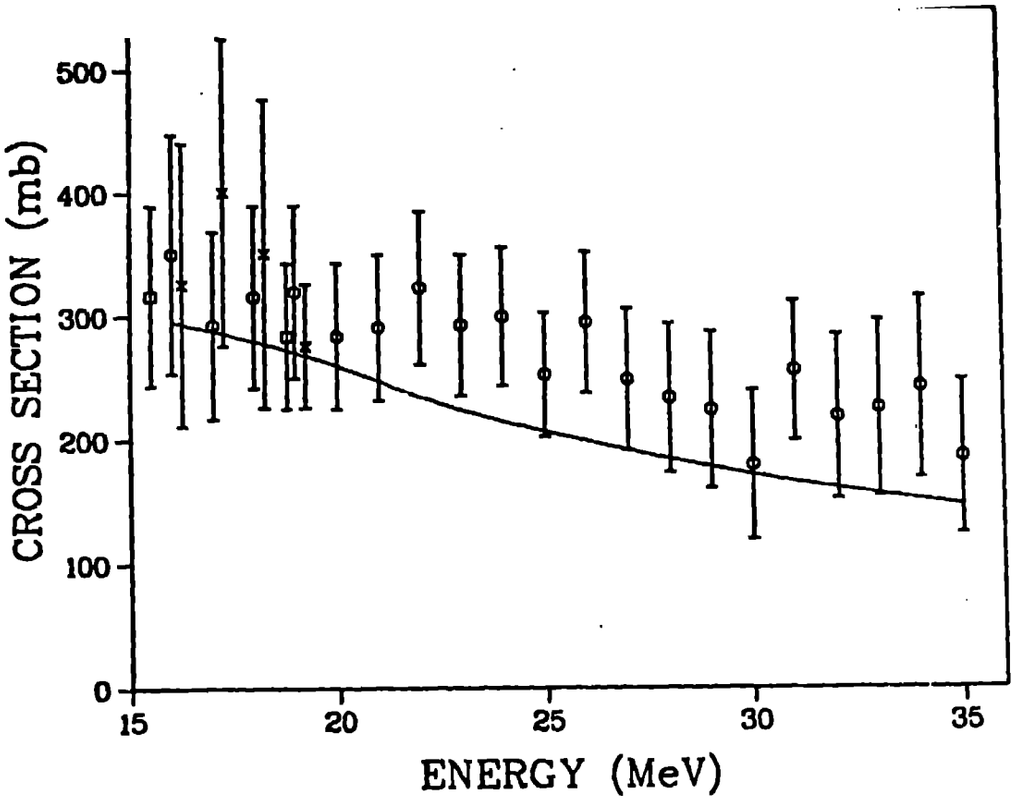
CROSS SECTION (mb)
500
400
300
200
100
0
15
20
25
30
35
ENERGY (MeV)

Fig 6

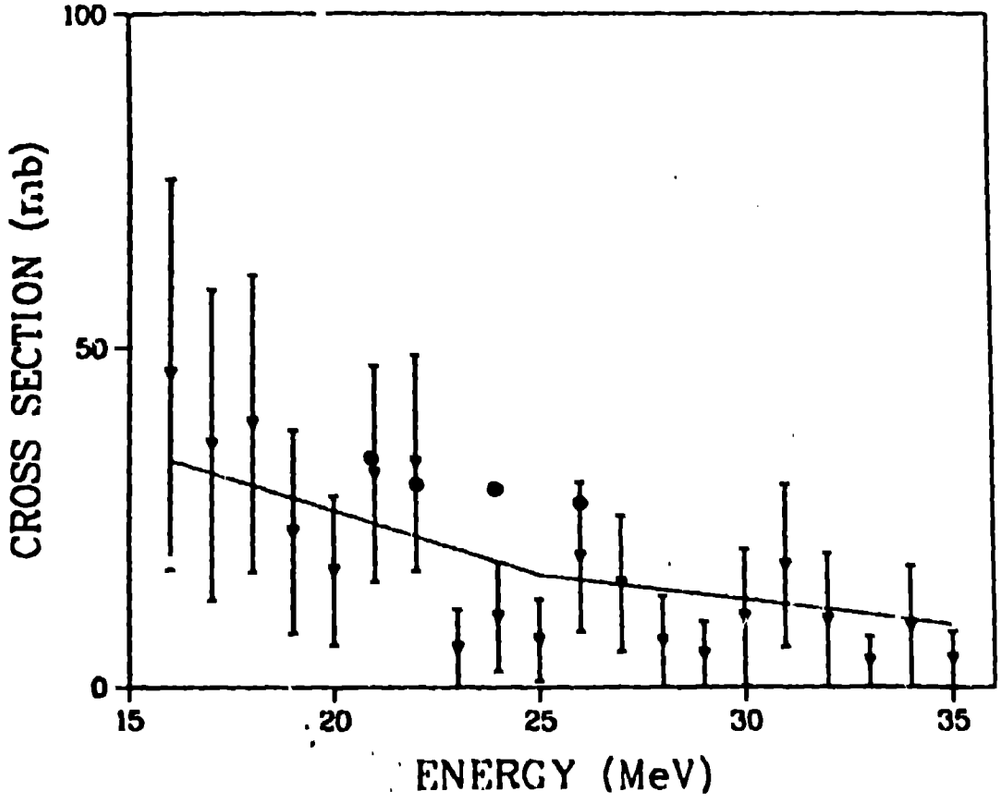
CROSS SECTION (mb)
100
50
0
15
20
25
30
35
ENERGY (MeV)

Fig 7

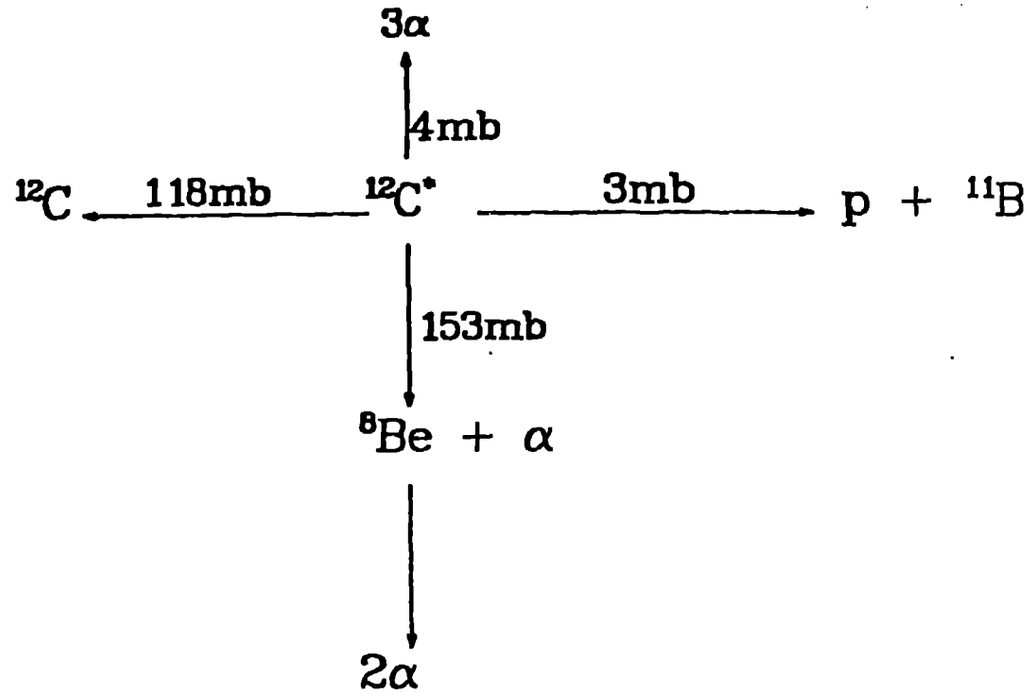
3α
4mb
12C
118mb
12C*
3mb
p + 11B
153mb
8Be + α
2α

Fig 8

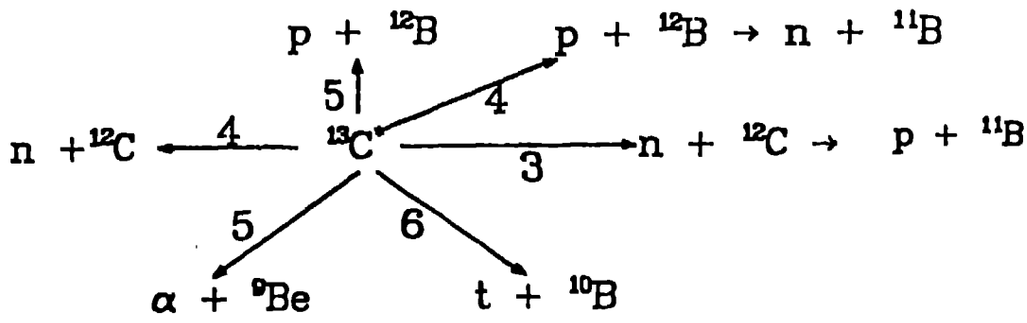
p + 12B
p + 12B → n + 11B
5
4
n + 12C
4
13C*
n + 12C → p + 11B
3
5
6
α + 9Be
t + 10B

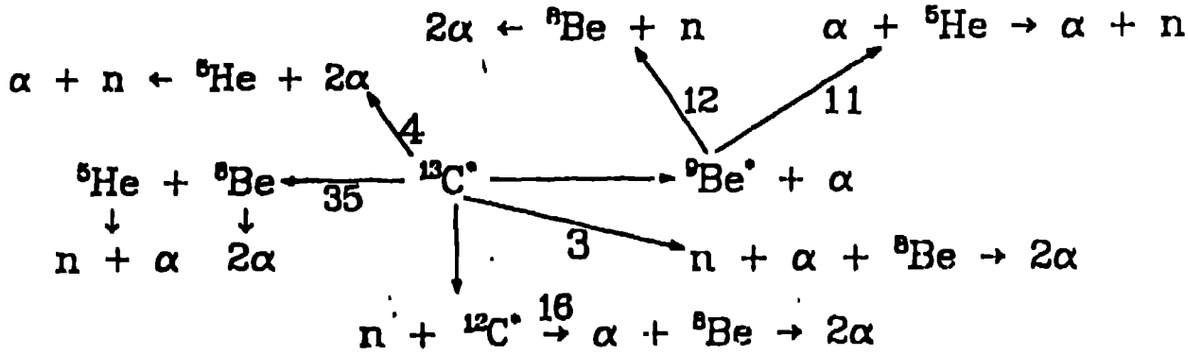
2α ← 8Be + n
α + 5He → α + n
α + n ← 5He + 2α
12
11
4
5He + 8Be
35
13C*
9Be* + α
n + α
2α
3
n + α + 8Be → 2α
n + 12C* 16 → α + 8Be → 2α

Fig 9

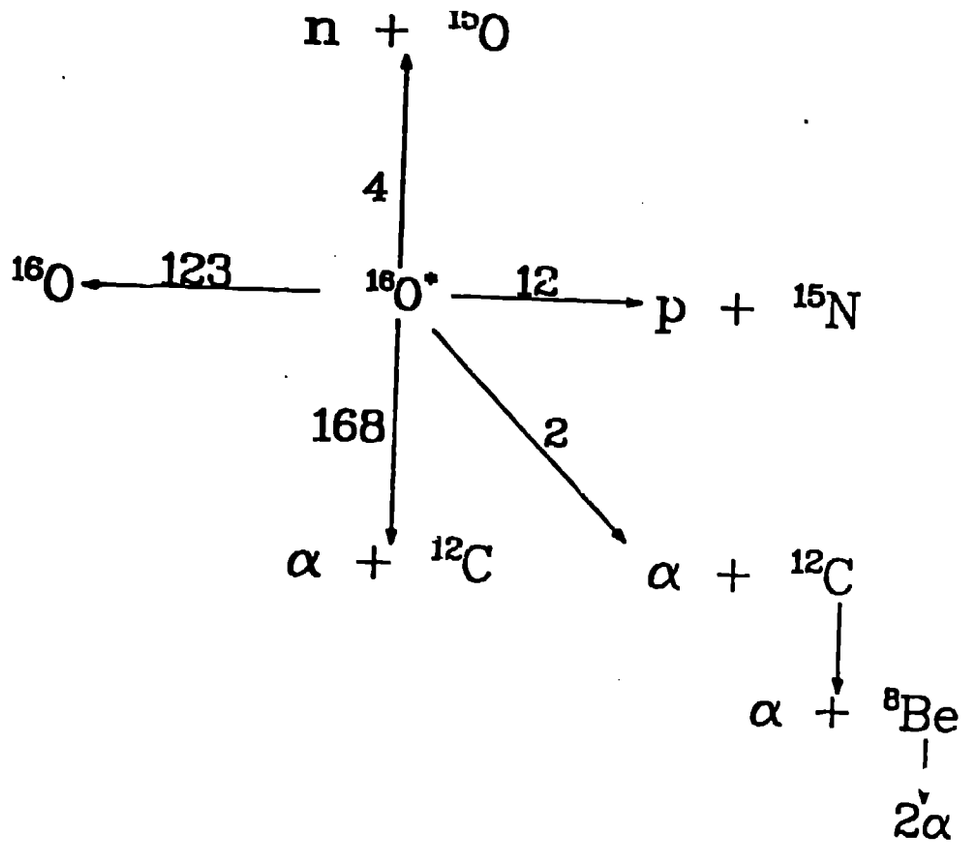
n + 15O
4
16O
123
16O*
12
p + 15N
168
2
α + 12C
α + 12C
α + 8Be
2α

Fig 10

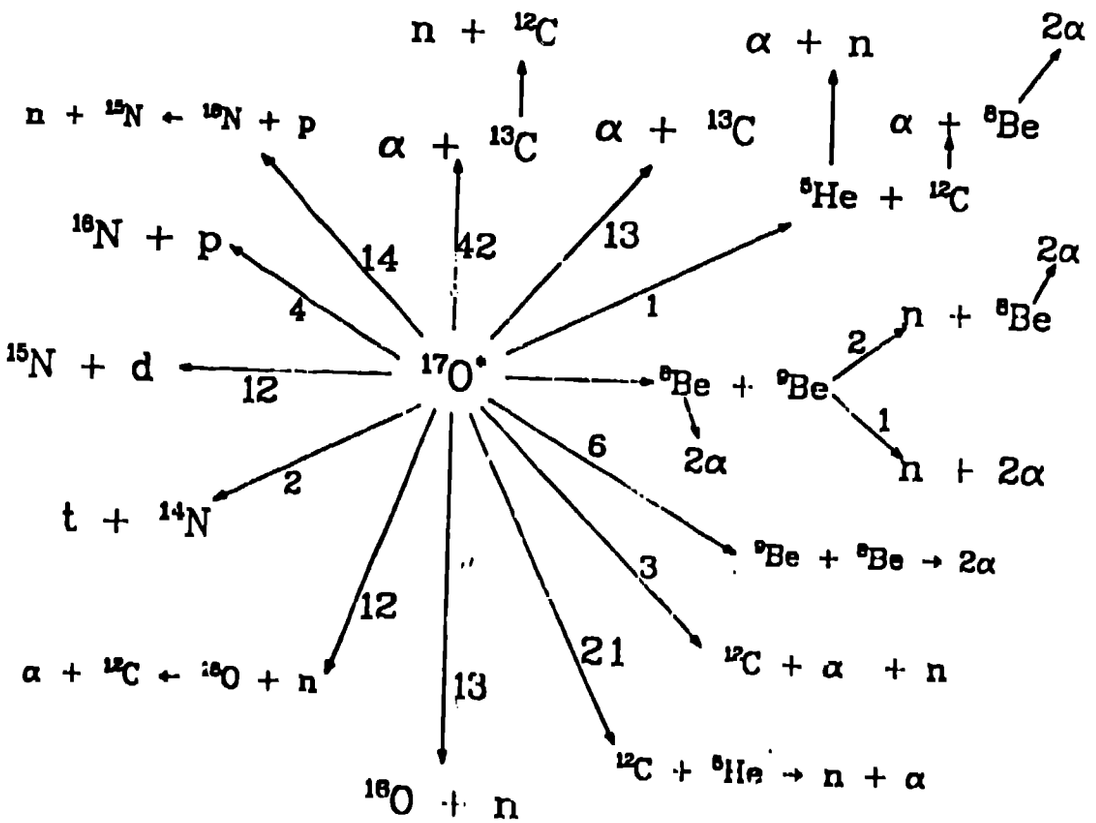
n + 12C
α + n
2α
n + 15N ← 16N + p
α + 13C
α + 13C
α + 8Be
5He + 12C
16N + p
14
42
13
1
2α
n + 8Be
2
15N + d
12
17O*
8Be + 9Be
1
n + 2α
2α
6
t + 14N
2
9Be + 8Be → 2α
3
12
21
α + 12C ← 16O + n
12C + α + n
13
12C + 5He → n + α
16O + n

Fig 11

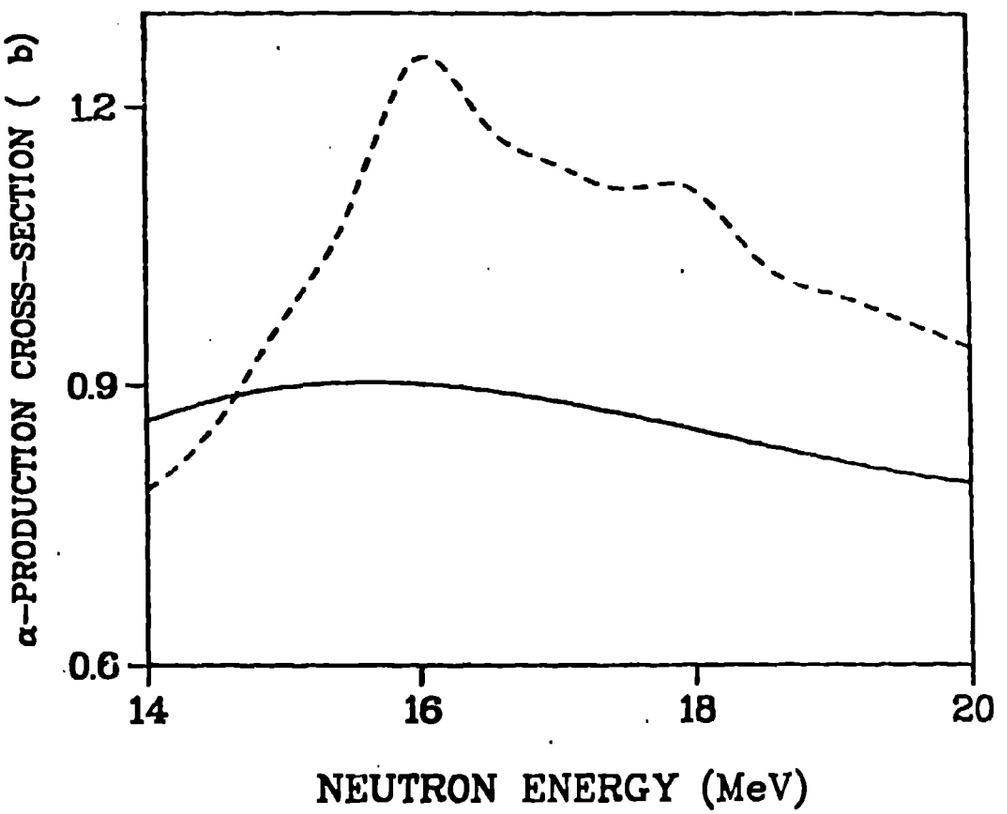
α-PRODUCTION CROSS-SECTION (b)
1.2
0.9
0.6
14
16
18
20
NEUTRON ENERGY (MeV)

Fig 12